The 2014 World Congress on
Advances in Civil, Environmental, and Materials Research (ACEM14)
Busan, Korea, August 24-28, 2014

Stress Intensity Factor Calculation for 2-D Cracked Bodies by Petrov-Galerkin Natural Element Method

*Jin-Rae Cho[1)]

[1)] *School of Mechanical Engineering, Pusan National University, Busan 609-735, Korea*
[1)] *jrcho@pusan.ac.kr*

ABSTRACT

This paper is concerned with the numerical calculation of stress intensity factors in 2-D linear fracture problems by Petrov-Galerkin natural element (PG-NE) method, for which Voronoi polygon-based Laplace interpolation functions and CS-FE basis functions are taken for the trial and test fuctions respectively. Conventional finite element method using CS-FE basis functions is also used for the comparison purpose, and the stress intensity factors of edge cracks are calculated by the interaction integral methods. It is observed that PG-NE method calculates the stress intensity factors more accurately than conventional finite element method using CS-FE basis functions.

1. INTRODUCTION

By virtue of the high calculation accuracy, but relatively easy numerical implementation, as well as the path-independence, the *J*-integral method has been widely used to calculate the stress intensity factors. In case of calculation by finite element method, the contour integral is usually recasted into an equivalent domain integral form, the interaction integral (Yau et al., 1980). The numerical calculation of stress intensity factors were traditionally made by either finite element method or boundary element method. But, since the late 1990s, the extension of meshfree methods to this problem have been actively progressed, in particular for the calculation by the interaction integral using the weighting function, inspired by the fact that the interpolation functions used in meshfree methods provide the high smoothness.

According to our brief literature survey, Belytschko et al. (1995) applied the element-free Galerkin (EFG) method to compute the singular stress fields and the stress intensity factors in 2-D fracture problems involving fatigue crack growth and dynamic crack propagation. Fleming et al. (1997) enriched the EFG method by adding asymptotic fields to the trial function and augmenting the basis function by the asymptotic fields, in order to accurately calculate stress intensity factors with fewer degrees of freedom. Ching and Batra (2001) enriched the polynomial basis functions in the meshless local Petrov-Galerkin (MLPG) method with the crack tip singular fields to predict the singular stress fields near a crack tip and stress intensity factors. Rao and

Rahman (2000; 2001) applied the EFG method to calculate the stress intensity factor and to simulate the crack propagation in 2-D linear fracture problems under mode-I and mixed-mode loading conditions, and also they introduced a coupled meshless-finite element method to reduce the computational effort. Fan et al. (2004) enriched the partition-of-unity (POU) method by embedding an analytical solution exactly describing the crack-tip stress field into the FE shape function to calculate the stress intensity factors of 2-D cracks.

As an extension of our previous work (2006a; 2006b; 2013), this paper intends to extend the natural element to the calculation of stress intensity factors of 2-D linear fracture problems. In order for the accurate and easy numerical integration using the Gauss quadrature rule, triangular constant-strain FE (CS-FE) basis functions are used for trial functions. The stress intensity factors of edge cracks under mode-I are calculated by the interaction integral method using Petrov-Galerkin natural element (PG-NE) method. In addition, the stress intensity factors are also calculated by the Bubanov-Galerkin natural element (BG-NE) method and standard finite element method.

2. 2-D LINEAR ELASTIC BODIE WITH CRACK

Referring to Fig. 1, let us consider a 2-D linear elastic body with a crack which occupies an open bounded domain $\Omega \in \Re^2$ with the boundary $\partial\Omega = \overline{\Gamma_D \cup \Gamma_N \cup \Gamma_c}$, where Γ_D denotes the displacement boundary, Γ_N the traction boundary, and $\Gamma_c = \overline{\Gamma_c^+ \cup \Gamma_c^-}$ the crack surfaces. For two-dimensional planar configurations, the rate of released energy per unit crack extension in the $x-$direction can be defined by the $J-$integral formulation given by

$$J = \int_\Gamma \left(W\delta_{1j} - \sigma_{ij} \frac{\partial u_i}{\partial x_1} \right) n_j ds \tag{1}$$

where $W = \boldsymbol{\sigma} \cdot \boldsymbol{\varepsilon} / 2$ is the strain energy density and σ_{ij} are Cauchy stresses evaluated along an arbitrary contour Γ enclosing the crack tip in a counter-clock wise sense. For a mixed-mode crack problem, J is related to the stress intensity factors such that $J = K_I^2 + K_{II}^2 / \bar{E}$ according to Irwin's relation (1957). In which $\bar{E}$ becomes E for plane stress state and $E/\left(1-\nu^2\right)$ for plane strain state, respectively.

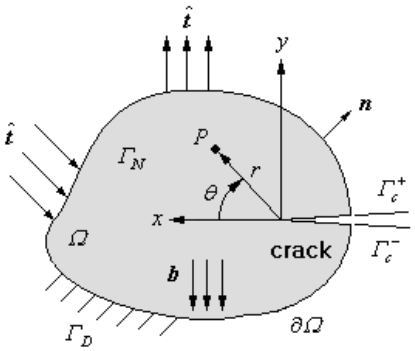

Fig. 1 A 2-D linear elastic body with an edge crack.

In order to extract K_I and K_{II}, the interaction integral (Yau et al., 1980; Shih and Asaro, 1988) which considers two equilibrium states of a cracked body is employed. State 1 is the actual equilibrium state of a body subject to the prescribed boundary conditions while state 2 denotes an auxiliary equilibrium state which will be chosen as the asymptotic fields for modes I or II. The interaction integral denoted by $M^{(1,2)}$ for the two equilibrium states is defined by

$$M^{(1,2)} = \int_{\Gamma} \left[W^{(1,2)} \delta_{1j} - \sigma_{ij}^{(1)} \frac{\partial u_i^{(2)}}{\partial x_1} - \sigma_{ij}^{(2)} \frac{\partial u_i^{(1)}}{\partial x_1} \right] n_j ds \tag{2}$$

where $W^{(1,2)}$ denotes the mutual strain energy defined by $W^{(1,2)} = \left[\boldsymbol{\sigma}^{(1)} \cdot \boldsymbol{\varepsilon}^{(2)} + \boldsymbol{\sigma}^{(2)} \cdot \boldsymbol{\varepsilon}^{(1)} \right] / 2$. Referring to Anderson (1991), the closed form near-tip displacement fields for modes I and II in two-dimensional linear fracture mechanics are available. And, the mode I stress intensity factor $K_I^{(1)}$ for state 1 can be determined by making state 2 as the pure mode I asymptotic field with $K_I^{(2)} = 1$:

$$M^{(1,\text{Mode I})} = \frac{2}{\overline{E}} K_I^{(1)} \tag{3}$$

In a similar manner, the stress intensity factor K_{II} of mode II can be also determined.

The line integral (2) is not best for numerical calculation because the integration of displacement gradients, strains and stresses of states 1 and 2 along path Γ is rather painstaking. Thus, it is desired to be transformed into an area integral form, for which Eq. (2) is firstly rewritten as

$$M^{(1,2)} = \int_{C} \left[\sigma_{ij}^{(1)} \frac{\partial u_i^{(2)}}{\partial x_1} + \sigma_{ij}^{(2)} \frac{\partial u_i^{(1)}}{\partial x_1} - W^{(1,2)} \delta_{1j} \right] q m_j ds \tag{3}$$

by substituting the path Γ with $C = \Gamma + \Gamma_c^- + \Gamma_c^+ + \Gamma_o$ as shown in Fig. 2 and multiplying a sufficiently smooth weighting function $q(\boldsymbol{x})$. It is not hard to realize that Eqs. (2) and (3) are equivalent when $q(\boldsymbol{x})$ becomes unity on Γ and vanishes on Γ_o, by assuming that the crack faces are traction free and straight in the darkened region A.

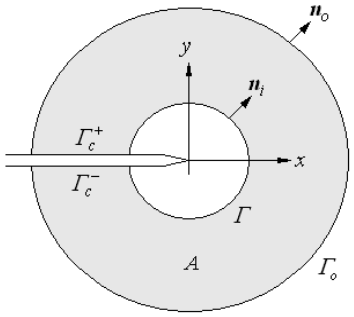

Fig. 2 An extended closed path and the integral domain A.

By taking the divergence theorem to Eq. (3) and letting the inner path Γ be shrunk to the crack tip, the transformed line integral (3) ends up with

$$M^{(1,2)} = \int_A \left[\sigma_{ij}^{(1)} \frac{\partial u_i^{(2)}}{\partial x_1} + \sigma_{ij}^{(2)} \frac{\partial u_i^{(1)}}{\partial x_1} - W^{(1,2)} \delta_{1j} \right] \frac{\partial q}{\partial x_j} dA \tag{4}$$

3. PETROV-GALERKIN NATURAL ELEMENT APPROXIMATION

The virtual work principle converts 2-D linear elasticity problem to the weak form: Find $\boldsymbol{u}(\boldsymbol{x})$ such that

$$\int_\Omega \boldsymbol{\varepsilon}(\boldsymbol{v}) : \boldsymbol{\sigma}(\boldsymbol{u}) d\Omega = \int_\Omega \boldsymbol{b} \cdot \boldsymbol{v} \, d\Omega + \int_{\Gamma_N} \hat{\boldsymbol{t}} \cdot \boldsymbol{v} \, ds \tag{5}$$

for every admissible displacement field $\boldsymbol{v}(\boldsymbol{x})$. In order for the Petrov-Galerkin natural element approximation using a given natural element grid $\Im_{NEM}$ composed of N nodes, trial and test displacement fields $\boldsymbol{u}(\boldsymbol{x})$ and $\boldsymbol{v}(\boldsymbol{x})$ are expanded as

$$\boldsymbol{u}^h(\boldsymbol{x}) = \sum_{J=1}^{N} \boldsymbol{u}_J \phi_J(\boldsymbol{x}) = \Phi \bar{\boldsymbol{u}} \,, \quad \boldsymbol{v}^h(\boldsymbol{x}) = \sum_{I=1}^{N} \boldsymbol{v}_I \psi_I(\boldsymbol{x}) = \Psi \bar{\boldsymbol{v}} \tag{6}$$

with Laplace interpolation functions $\phi_J(\boldsymbol{x})$ and CS-FE basis functions $\psi_I(\boldsymbol{x})$. In addition, Φ and Ψ are $(2 \times 2N)$ matrices containing N basis functions ϕ_J and ψ_I, and $\bar{\boldsymbol{u}}$ and $\bar{\boldsymbol{v}}$ denote the $(2N \times 1)$ nodal vectors, respectively.

Introducing Eq. (6) into Eq. (5) leads to

$$\sum_I^N \boldsymbol{K}^I \bar{\boldsymbol{u}} = \sum_I^N \boldsymbol{F}^I \tag{7}$$

with the node-wise matrices defined by

$$\boldsymbol{K}^I = \int_{\Omega_v^I} (\boldsymbol{L}\Psi)^T \boldsymbol{E} (\boldsymbol{L}\Phi) d\Omega \tag{8}$$

$$\boldsymbol{F}^I = \int_{\Omega_v^I} \Psi^T \boldsymbol{b} \, d\Omega + \int_{\Gamma_N \cap \Omega_v^I} \Psi^T \hat{\boldsymbol{t}} \, ds \tag{9}$$

with $\Omega_v^I = supp(\psi_I(\boldsymbol{x}))$. Furthermore, $\boldsymbol{D}$ is the (3×2) divergence-like operator defining Cauchy strain tensor and $\boldsymbol{E}$ indicated the (3×3) material constant matrix of linear elasticity. It is noted that the numerical integration in natural element methods is carried out over the support of each test basis function.

Differing from the Buvnov-Galerkin natural element method (BG-NEM) in which Laplace interpolation functions $\phi_J(\boldsymbol{x})$ are used for the test function as well as for the trial function, the Petrov-Galerkin natural element method (PG-NEM) in the current study uses the Delaunay triangle-based basis functions to expand the test displacement field. By employing this kind of PG-NEM, we intend to achieve both the accuracy and implementation easiness in the numerical integration using conventional Gauss quadrature (Cho and Lee, 2006c). The numerical integration in most meshfree

methods is usually performed by applying the conventional Gauss quadrature rule to the background mesh which is additionally constructed. Contrary to the other meshfree methods, additional effort to construct a background mesh is not needed for PG-NEM because Delaunay triangles generated a priori in the process for defining the Laplace interpolation functions serve as a background mesh.

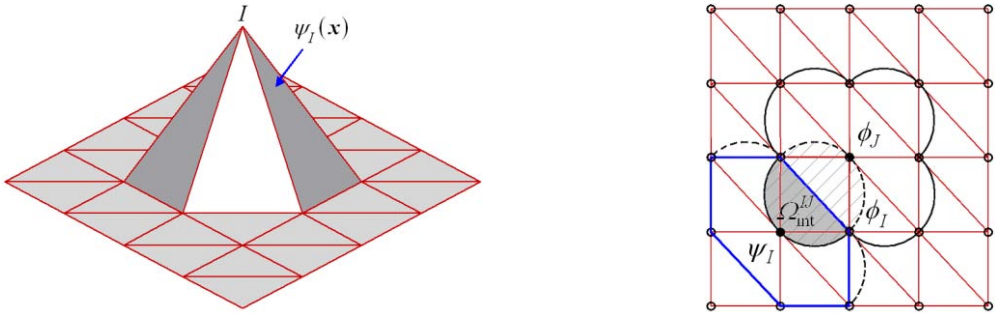

(a) (b)

Fig. 3 In the PG-NE method: (a) CS-FE basis function; (b) intersection region Ω_{int}^{IJ} between trial function $\phi_J(x)$ and test function $\psi_I(x)$.

4. COMPUTATION OF THE INTERACTION INTEGRAL

The integral domain A and the weighting function $q(x)$ for the interaction integral (4) are constructed by specifying a domain defining circle of radius r_{int} as shown in Fig. 4. The value of unity is assigned to all the nodes within the circle, while the value of zero is specified to the remaining nodes within a NEM grid. Then, a union of interior darkened eight Delaunay triangles generates a rectangular and its boundary serves as an interior path Γ shown in the previous Fig. 2. In addition, one can define another union of grayed Delaunay triangles in which only one or two nodes have the value of unity, and its boundary becomes the outer path Γ_o. Hence, the union of grayed Delaunay triangles automatically becomes the integral domain A, where the weighting function $q(x)$ has the value between zero and unity.

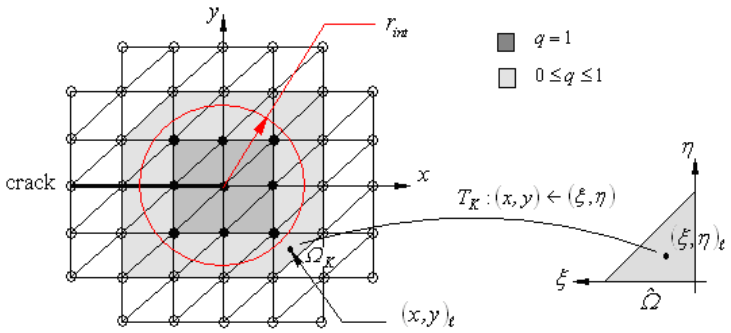

Fig. 4 The construction of the integral domain A and the weighting function $q(x)$.

Referring to Fig. 4, the gradient of weighting function vanishes outside the integral domain A. So, let us denote M_A be the total number of grayed Delaunay triangles in

the integral domain A. Then, the interaction integral (4) is integrated triangle by triangle such that

$$M^{(1,2)} = \sum_{K=1}^{M_A} M_K^{(1,2)} \tag{10}$$

with $M_K^{(1,2)}$ being the triangle-wise interaction integrals. Here, each triangle-wise interaction integral is computed by

$$\begin{aligned} M_e^{(1,2)} &= \int_{\Omega_K} \left[\sigma_{ij}^{(1)} \frac{\partial u_i^{(2)}}{\partial x_1} + \sigma_{ij}^{(2)} \frac{\partial u_i^{(1)}}{\partial x_1} - W^{(1,2)} \delta_{1j} \right] \frac{\partial q}{\partial x_j} dA \\ &= \sum_{\ell=1}^{INT} \left[\sigma_{ij}^{(1)} \frac{\partial u_i^{(2)}}{\partial x_1} + \sigma_{ij}^{(2)} \frac{\partial u_i^{(1)}}{\partial x_1} - W^{(1,2)} \delta_{1j} \right]_{\boldsymbol{x}_\ell} \left. \frac{\partial q}{\partial x_j} \right|_{\boldsymbol{x}_\ell} w_\ell \left| \boldsymbol{J} \right|_{\boldsymbol{x}_\ell} \end{aligned} \tag{11}$$

using Gauss quadrature rule, in which INT, $\boldsymbol{x}_\ell$ and w_ℓ indicate the total number of integration points, sampling points and weights, respectively. Note that the sampling points $\boldsymbol{x}_\ell$ in Ω_K and the Jacobian $\left|\boldsymbol{J}\right|_{\boldsymbol{x}_\ell}$ are calculated using the geometry transformation T_K defined by

$$T_K : x_\ell = \sum_{i=1}^{3} x_i \psi_i(\xi,\eta)_\ell, \quad y_\ell = \sum_{i=1}^{3} y_i \psi_i(\xi,\eta)_\ell \tag{12}$$

between Ω_K and the master triangle element $\hat{\Omega}$. Here, $\{x_i, y_i\}$ are the co-ordinates of three grid points in each Delaunay triangle, $(\xi,\eta)_\ell$ the Gauss points in $\hat{\Omega}$, and ψ_i the basis functions. For the current study, two kinds of basis functions are used to interpolate the weighting function $q(\boldsymbol{x})$, CS-FE basis and Laplace interpolation function.

In two-dimensional fracture problems, the displacement and stress fields at the tip of a mixed mode crack which are used for state 2 are given by (Anderson, 1991)

$$\begin{Bmatrix} u_x(\boldsymbol{x}) \\ u_y(\boldsymbol{x}) \end{Bmatrix} = \frac{K_I}{2G}\sqrt{\frac{r}{2\pi}} \begin{Bmatrix} cos\frac{\theta}{2}\left[\kappa - 1 + 2sin^2\frac{\theta}{2}\right] \\ sin\frac{\theta}{2}\left[\kappa + 1 - 2cos^2\frac{\theta}{2}\right] \end{Bmatrix} + \frac{K_{II}}{2G}\sqrt{\frac{r}{2\pi}} \begin{Bmatrix} sin\frac{\theta}{2}\left[\kappa + 1 + 2cos^2\frac{\theta}{2}\right] \\ -cos\frac{\theta}{2}\left[\kappa - 1 - 2sin^2\frac{\theta}{2}\right] \end{Bmatrix} \tag{13}$$

$$\begin{Bmatrix} \sigma_x(\boldsymbol{x}) \\ \sigma_y(\boldsymbol{x}) \\ \sigma_{xy}(\boldsymbol{x}) \end{Bmatrix} = \frac{K_I}{\sqrt{2\pi r}} cos\frac{\theta}{2} \begin{Bmatrix} 1 - sin\frac{\theta}{2}sin\frac{3\theta}{2} \\ 1 + sin\frac{\theta}{2}sin\frac{3\theta}{2} \\ sin\frac{\theta}{2}cos\frac{3\theta}{2} \end{Bmatrix} + \frac{K_{II}}{\sqrt{2\pi r}} \begin{Bmatrix} -sin\frac{\theta}{2}\left(2 + cos\frac{\theta}{2}cos\frac{3\theta}{2}\right) \\ sin\frac{\theta}{2}cos\frac{\theta}{2}cos\frac{3\theta}{2} \\ cos\frac{\theta}{2}\left(1 - sin\frac{\theta}{2}sin\frac{3\theta}{2}\right) \end{Bmatrix} \tag{14}$$

Where, r is the distance from the crack tip to the observation point $\boldsymbol{x}$ and θ is the angle from the tangent to the crack path. And, G is the shear modulus κ is the Kolosov constant defined by $\kappa = (3-\nu)/(1+\nu)$ for plane stress condition and $\kappa = (3-4\nu)$

for plane strain condition respectively,

5. NUMERICAL EXPERIMENTS

We consider a rectangular plate in plane-strain state with edge crack as shown in Fig. 5(a), where the width b and the height $2h$ are $1.0in$ and $2.0in$ and uniform tensile distributed load $\sigma = 1.0psi$ is applied to the top and bottom sides. The bottom left corner is simply supported and the bottom right corner is clamped, and Young's modulus E and Poisson's ratio ν are set by 1.0×10^3 and 0.3 respectively. The plate domain is uniformly discretized as shown in Figs. 5(b) and 13 Gaussian points are used. For the purpose of comparison, the stress intensity factors are also calculated by finite element method using CS-FE triangular elements. The crack length is set variable and the radius r_{int} of domain defining circle is basically set by two times of the square of the area of a rectangular element composed of two Delaunay triangles (Moës et al., 1999).

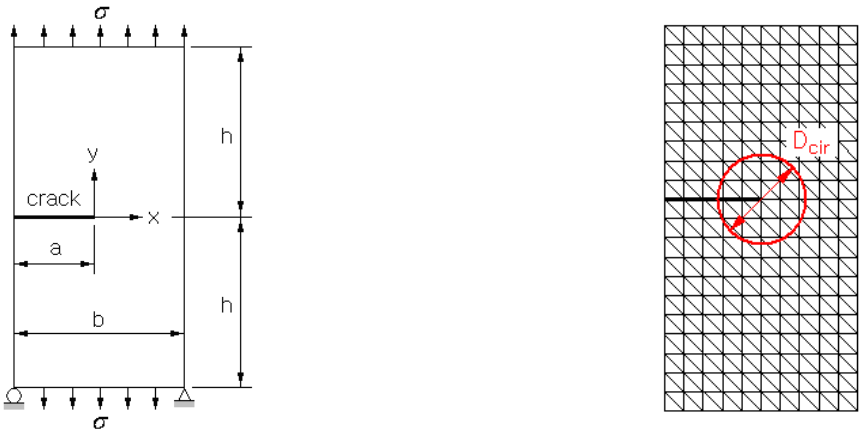

(a) (b)

Fig. 5 (a) A rectangular plate with edge crack under uniform tension, (b) NEM grid.

According to Tada et al. (1973), the reference stress intensity factors K_I of mode I are given by $K_I = \sigma\sqrt{\pi a}\, f(a/b)$ with a being the crack length and $f(a/b)$ being an empirical function defined by

$$f\left(\frac{a}{b}\right) = 1.12 - 0.231\left(\frac{a}{b}\right) + 10.55\left(\frac{a}{b}\right)^2 - 21.72\left(\frac{a}{b}\right)^3 + 30.39\left(\frac{a}{b}\right)^4 \tag{15}$$

for $a/b \le 0.6$. The stress intensity factors K_I calculated by three different methods using uniform 21×41 grid points for seven different relative crack lengths a/b are recorded in Table I and represented in Fig. 6(a). It is observed that PG-NE method provides the highest numerical accuracy and its prediction accuracy increases in proportional to the crack length such that the relative error with respect to the exact value is 2.70% at the relative crack length of $a/b = 0.5$. Meanwhile, the difference in the prediction accuracy between PG-NE2 and CS-FE methods is negligible, but PG-NEM2 provides slightly higher accuracy at larger crack length.

Table I. Stress intensity factors K_I to the relative crack length (21×41 grid points).

Methods	Relative crack length (a/b)						
	0.2	0.25	0.3	0.35	0.4	0.45	0.5
Exact	1.0865	1.3302	1.611	1.9465	2.3580	2.8766	3.5423
PG-NEM	0.7972 (-26.63%)	1.0394 (-21.86%)	1.3333 (-17.26%)	1.7027 (-12.53%)	2.1775 (-7.66%)	2.8009 (-2.63%)	3.6381 (+2.70%)
PG-FEM2*	0.2267 (-79.13%)	0.3463 (-73.96%)	0.5662 (-64.87%)	0.7406 (-61.96%)	1.0524 (-55.37%)	1.4821 (-48.48%)	2.0828 (-41.20%)
CS-FEM	0.2428 (-77.65%)	0.3531 (-73.45%)	0.5608 (-65.20%)	0.7189 (-63.07%)	1.0065 (-57.32%)	1.4006 (-51.31%)	1.9474 (-45.02%)

(*) indicates the PG-NE method in which the weighting function is interpolated with CS-FE basis functions.

Table II and Fig. 6(b) represent the numerical results obtained using uniform 41×81 grid points, where one can realize that all three methods provide the stress intensity factors with larger relative errors. Since the radius r_{int} of domain defining circle is set by two times of the square of the area of a rectangular element composed of two Delaunay triangles, it becomes smaller by two times when compared with the numerical results obtained using 21×41 grid points. And, it can be inferred that the smaller integration domain negatively influences the stress intensity calculation from the fact of common deterioration in the numerical prediction accuracy of all three methods.

Table III. Stress intensity factors K_I to the relative crack length (41×81 grid points).

Methods	Relative crack length (a/b)						
	0.2	0.25	0.3	0.35	0.4	0.45	0.5
Exact	1.0865	1.3302	1.611	1.9465	2.3580	2.8766	3.5423
PG-NEM	0.7676 (-29.35%)	0.9821 (-26.17%)	1.2434 (-22.84%)	1.5691 (-19.39%)	1.9838 (-15.87%)	2.5229 (-12.30%)	3.2400 (-8.53%)
PG-FEM2	0.1661 (-84.71%)	0.2534 (-80.95%)	0.3744 (-76.77%)	0.5401 (-72.25%)	0.7669 (-67.48%)	1.0796 (-62.47%)	1.6769 (-52.66%)
CS-FEM	0.2534 (-83.17%)	0.2665 (-79.97%)	0.3827 (-76.25%)	0.5421 (-72.15%)	0.7600 (-67.77%)	1.0600 (-63.15%)	1.4787 (-58.26%)

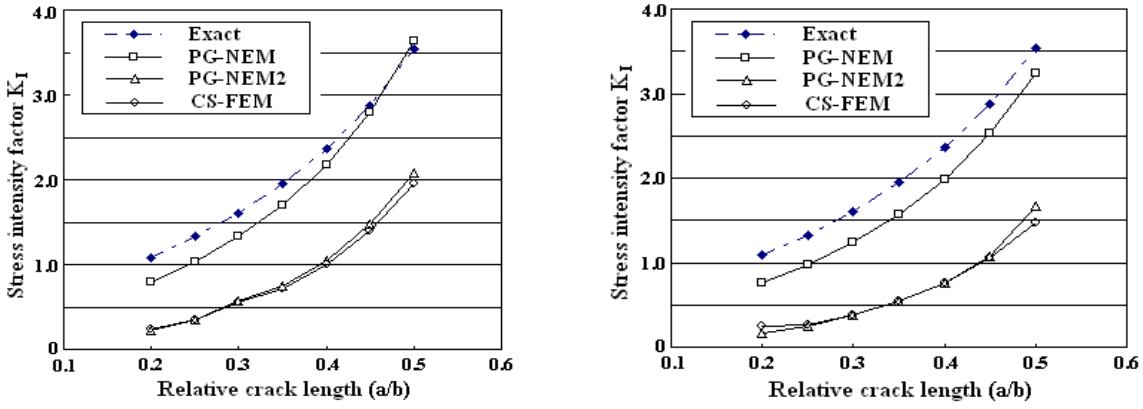

(a) (b)

Fig. 6 SIFs K_I for three different methods: (a) 21×41 grid points, (b) 41×81 grid points.

CONCLUSION

An extension of Petrov-Galerkin natural element method (PG-NEM) to 2-D linear structural and fracture mechanics with high stress singularity has been addressed in this paper, in order to explore its characteristics in aspect of the numerical accuracy. The interaction integral method was formulated by PG-NEM to calculate the stress intensity factors of edge cracks, for which a L^2-projection stress recovery technique was employed to obtain more accurate smothered strain and stress fields. For the comparison purpose, the stress intensity factors were also calculated by CS-FE and PG-NE2 methods in which the weighting function is defined by CS-FE basis functions. Through the numerical experiment, it has been clearly justified that PG-NEM provides more accurate and stable numerical results than the other methods.

REFERENCES

Anderson, T.L. (1991) *Fracture Mechanics: Fundamentals and Applications*, 1st edition, CRC Press.

Belytschko, T., Lu, Y.Y., Gu, L., Tabbara, M. (1995) “Element-free Galerkin methods for static and dynamic fracture,” *International Journal of Solids and Structures* **32**(17-18):2547-2570.

Ching, H.K., Batra, R.C. (2001) “Determination of crack tip fields in linear elastostatics by the meshless local Petrov-Galerkin (MLPG) method,” *Computer Modeling in Engineering and Science* **2**(2):273-289.

Cho, J.R., Lee, H.W. (2006a) “A Petrov-Galerkin natural element method securing the numerical integration accuracy,” *Journal of Mechanical Science and Technology* **20**(1):94-109.

Cho, J.R., Lee, H.W. (2006b) “2-D large deformation analysis of nearly incompressible body by natural element method,” *Computers and Structures* **84**:293-304.

Cho, J.R., Lee, H.W. (2006c) “2-D frictionless dynamic contact analysis of large deformable bodies by Petrov-Galerkin natural element method,” *Computers and Structures* **85**:1230-1242.

Cho, J.R., Lee, H.W., Yoo, W.S. (2013) “Natural element approximation of Reissner-Mindlin plate for locking-free numerical analysis of plate-like thin elastic structures,” *Computer Methods in Applied Mechanics and Engineering* **256**:17-28.

Fan, S.C., Liu, X., Lee, C.K. (2004) “ Enriched partition-of-unity finite element method for stress intensity factors at crack tips,” *Computers and Structures* **82**:445-461.

Fleming, M., Chu, Y.A., Moran, B., Belytschko, T. (1997) “Enriched element-free Galerkin methods for crack tip fields,” *International Journal for Numerical Methods in Engineering* **40**:1483-1504.

Irwin, G.R. (1957) “Analysis of stresses and strains near the end of a crack traveling a plate,” *Journal of Applied Mechanics* **24**:361-364.

Moës, N., Dolbow, J., Belytschko, T. (1999) “A finite element method for crack growth without remeshing,” *International Journal for Numerical Methods in Engineering* **46**:131-150.

Rao, B.N., Rahman, S. (2000) “An efficient meshless method for fracture analysis of cracks,” *Computational Mechanics* **26**:398-408.

Rao, B.N., Rahman, S. (2001) “A coupled meshless-finite element method for fracture analysis of cracks,” *International Journal of Pressure Vessels and Piping* **78**:647-657.

Shih, C.F., Asaro, R.J. (1988) “Elasto-plastic analysis of cracks on biomaterial interfaces: Part I – small scale yielding,” *Journal of Applied Mechanics* **55**:299-316.

Tada, H., Paris, P.C., Irwin, G.R. (1973) *The Stress Analysis of Cracks Handbook*, Del Research Corporation, Hellertown, PA.

Yau, J.F., Wang, S.S., Corten, H.T. (1980) “A mixed-mode crack analysis of isotropic solids using conservation laws of elasticity,” *Journal of Applied Mechanics* **47**:335-341.